BMES
BIOMEDICAL ENGINEERING SOCIETY™
www.bmes.org

CrossMark

Measurement of Strain in Cardiac Myocytes at Micrometer Scale Based on Rapid Scanning Confocal Microscopy and Non-Rigid Image Registration

J. Lichter,[1,2] Hui Li,[1] and Frank B. Sachse[1,2]

[1]Nora Eccles Harrison Cardiovascular Research and Training Institute, University of Utah, 95 South 2000 East, Salt Lake City, UT 84112-5000, USA; and [2]Department of Bioengineering, University of Utah, Salt Lake City, UT 84112, USA

Associate Editor Ellen Kuhl oversaw the review of this article.

Abstract—Measurement of cell shortening is an important technique for assessment of physiology and pathophysiology of cardiac myocytes. Many types of heart disease are associated with decreased myocyte shortening, which is commonly caused by structural and functional remodeling. Here, we present a new approach for local measurement of 2-dimensional strain within cells at high spatial resolution. The approach applies non-rigid image registration to quantify local displacements and Cauchy strain in images of cells undergoing contraction. We extensively evaluated the approach using synthetic cell images and image sequences from rapid scanning confocal microscopy of fluorescently labeled isolated myocytes from the left ventricle of normal and diseased canine heart. Application of the approach yielded a comprehensive description of cellular strain including novel measurements of transverse strain and spatial heterogeneity of strain. Quantitative comparison with manual measurements of strain in image sequences indicated reliability of the developed approach. We suggest that the developed approach provides researchers with a novel tool to investigate contractility of cardiac myocytes at subcellular scale. In contrast to previously introduced methods for measuring cell shorting, the developed approach provides comprehensive information on the spatio-temporal distribution of 2-dimensional strain at micrometer scale.

Keywords—Cardiac myocyte, Contraction, Strain, Non-rigid image registration.

ABBREVIATIONS

DHF	Dyssynchronous heart failure
EC	Excitation–Contraction

Address correspondence to Frank B. Sachse, Nora Eccles Harrison Cardiovascular Research and Training Institute, University of Utah, 95 South 2000 East, Salt Lake City, UT 84112-5000, USA. Electronic mail: frank.sachse@utah.edu

INTRODUCTION

Efficient pump function of the heart requires concerted contraction of cardiac muscle cells (myocytes). Contraction is commonly initiated by electrical activation of the myocytes. The term excitation–contraction (EC) coupling refers to the signaling cascade transducing electrical activation into mechanical contraction and is based on calcium signaling.[3] EC coupling in cardiac myocytes is initiated by a small influx of calcium through the membrane (sarcolemma), which triggers calcium release from an intracellular calcium store, the sarcoplasmic reticulum, into the cytosol. The calcium diffuses within the cell. Binding of calcium to the protein troponin C allows interactions of actin and myosin filaments, which generate force and induce cell shortening. The actin and myosin filaments are located in sarcomeres, which are the contractile units within cardiac myocytes.

Isolated cardiac myocytes are a major experimental preparation to study physiological mechanisms underlying contraction. Also, isolated myocytes are a major research tool to investigate structural and functional alterations by drugs and diseases. Several methods have been introduced to measure mechanical contraction in these cells. Early approaches for measurement of contraction were based on transmitted light microscopy and analysis of 1- or 2-dimensional image sequences. Tameyasu *et al.* used retrospective visual inspection of image sequences acquired at a frame rate of 200 Hz to measure segmental shortening in frog cardiac myocytes.[27] Several groups developed approaches based on 1-dimensional photodiode arrays and automated cell length detection from photodiode array data acquired at a rate of up to 1 kHz.[11,15,18]

Steadman *et al.* introduced a video-based device that applied an edge-detector to measure myocyte shortening at a frame rate of 60 Hz.[26] Further measurement approaches employed light diffraction to measure sarcomere length.[9,12] Diffraction instruments commonly apply a laser as a light source and have a spatial resolution of several nanometers per half sarcomere. Light diffraction methods can be applied to single cells and multicellular preparations. These methods provide 1-dimensional information on Z-line spacing and changes of this spacing during contraction. Recently developed approaches use confocal and 2-photon microscopy for measurement of cell contraction. Analysis of Fourier transformed image data determined the changes of sarcomere length.[4,16]

A typical measure of contraction is myocyte shortening λ, which is defined as:

$$\lambda = \frac{l}{l_0} \tag{1}$$

with the cell length at rest l_0 and the length in the contracted state l. Commonly, shortening is presented in percentage. An alternative measure of contraction is the Cauchy (or engineering) strain e defined as:

$$e = \frac{l - l_0}{l_0}. \tag{2}$$

Similar 1-dimensional measures have been established for quantifying shortening of sarcomeres.

While the described approaches yielded valuable insights into myocyte contraction, they only provide 1-dimensional information on contraction of cells or sarcomeres and do not yield information on transverse strain in response to contraction. Furthermore, the approaches lack high spatial resolution, which makes it difficult to characterize subcellular heterogeneities.

Here we introduce a new approach for local measurement of 2-dimensional strain within cells at a high spatial resolution. We developed the approach based on studies of synthetic cells and paced isolated myocytes from the left ventricle of canine hearts. We used cells from control animals and animals with dyssynchronous heart failure (DHF), which is thought to lead to severe remodeling of structures and functions associated with EC coupling and contraction.[2,5,13,14,21] Our approach is based on fluorescent labeling of the sarcolemma. Many types of myocytes exhibit a specialization of the sarcolemma, the transverse tubular system (t-system), which serves as the major initiation site for EC coupling. Our approach takes advantage of the spatial distribution of sarcolemma including t-system within myocytes, which is imaged using rapid-scanning confocal microscopy at high spatiotemporal resolution. We applied a previously developed method for non-rigid image registration to obtain a transformation describing the deformation between sequential frames of contracting myocytes.[19] We used this transformation to quantify the local displacement and strain within the myocyte during contraction. Finally, we evaluated the approach by comparison with manual measurements of strain.

MATERIALS AND METHODS

Animal Model and Cell Preparation

Animal studies complied with the *Guide for the Use and Care of Laboratory Animals* published by the National Institute of Health. All procedures were approved by the Animal Care and Use Committees of the University of Utah.

The animal model and methods for cell isolation have been previously described.[5,6,13,14,21] Briefly, mongrel canines were used as control and DHF models. DHF animals underwent pacemaker implantation with the pacing lead introduced through the jugular vein and anchored in the right ventricular apex. DHF was achieved by tachypacing in the right ventricle at 180–200 BPM for 6 weeks. Success of the model was determined by weekly ECGs and acquisition of hemodynamic data at the time of device implantation and harvesting of cells. We provide a description of our protocol for cell isolation in the supplemental data.

Confocal Imaging and Image Processing

Isolated cells were incubated with 12.5 μM of the Ca^{2+} sensitive dye Fluo-4 AM (Invitrogen, Grand Island, NY, USA) for 20 min. Cells were then exposed to 6.25 μM of the membrane staining dye Di-8-Anepps (Invitrogen) for 8 min. The cells were allowed to settle on the glass slide of a perfusion chamber attached to a Zeiss LSM 5 Live Duo confocal microscope equipped with a 63$\times$ oil immersion objective. The bath chamber was held at 37 °C and perfused with a modified Tyrode's solution containing 2 or 4 mM Ca^{2+}. In some cases 1 μM isoproterenol (Iso), a non-selective beta-adrenergic agonist, was added to the 4 mM Ca^{2+} solution to simulate beta-adrenergic stimulation. A 489 nm wavelength emitting diode laser was used to excite both dyes simultaneously. Emitted light was filtered using a dichromatic mirror with a cutoff wavelength of 535 nm and bandpass filters of 505–610 and 560–675 nm to split the Fluo-4 and Di-8-Anepps signals, respectively. Cells were field stimulated using a current amplitude of 10 mA. The cells were conditioned with a train of at least 10 stimuli at 0.5 Hz.

Image acquisition was triggered 20–40 ms prior to the final stimulus. Sequences of 100 2-dimensional images with a size of 128 × 1024 pixels were acquired at a frame rate of 4.6 ms/frame. Pixel sizes were 0.1 × 0.1 μm. Imaging was restricted to cells exhibiting clear striations and a regular brick shape. Example images acquired from a control cell are shown in Fig. 1a. Images from a control cell in the presence of isoproterenol and a DHF cell are presented in Supplemental Figs. 1a and c, respectively.

Low frequency noise in Fluo-4 and Di-8-Anepps images was filtered using Fourier transform. Crosstalk in the two images was calculated and removed from the Di-8-Anepps signal as previously described.[23] Noise reduction and background removal of the Di-8-Anepps signal was performed by filtering with a discretized 2D mean free Gaussian filter (13 × 13 pixels, $\sigma_x = \sigma_y = 0.2$ μm). A mask of the cell interior was created using predefined seed points and the watershed-based method previously described.[24] The cell mask defined a region of interest for subsequent analysis, allowing for the removal of extracellular debris and segments from other cells. Results of this preprocessing on the control cell, control cell in the presence of isoproterenol and DHF cell are presented in Figs. 1b–1d, respectively. Additional examples for this processing are provided in Supplemental Fig. 1. The cell mask, a manually defined angle of orientation and a semi-automatically selected endpoint were used to create a Euclidean distance map from the cell end. We used the combination of the cell mask and distance map to create regions of interest for the registration algorithm.

Manual Strain Measurement

Manual strain measurement of cells was performed in raw image sequences using ImageJ (v1.48).[22] In an image of a cell at rest, a line with a width of 8 pixels was drawn parallel to the longitudinal axis of the cell, while intersecting the cell end and several t-tubules (Fig. 2a). A second line was drawn intersecting the same structural landmarks of the cell in the image at peak contraction (Fig. 2c). The profiles of these two lines were examined (Figs. 2b and 2d) and local intensity maxima corresponding to the cell end and t-tubules identified. The maxima locations were used to calculate distances at rest and peak contraction. These distances were then used to calculate the Cauchy strain (Eq. 2).

Synthetic Cells

Based on knowledge of geometry and microstructure of ventricular myocytes we generated cross-sectional images of synthetic cells undergoing homogeneous contraction. The synthetic cells had a brick shape with a resting length, width and height of 100, 15 and 15 μm, respectively. Cells were assumed to be iso-volumetric during contraction and exhibiting transversely isotropic mechanical properties. Thus, for a given longitudinal strain $\varepsilon_{\text{Long}}$, the transverse strain $\varepsilon_{\text{Trans}}$ was calculated as

$$\varepsilon_{\text{Trans}} = \sqrt{\frac{1}{(1 + \varepsilon_{\text{Long}})}} - 1. \qquad (3)$$

Cells were modeled to have a $\varepsilon_{\text{Long}}$ of −10% at maximal contraction, which results in a length and width of 90 and 15.8 μm, respectively. The final $\varepsilon_{\text{Long}}$ of −10% was achieved in 10 linear steps, each at 1% contraction of the original image. We assumed a homogeneous distribution of t-tubules at a spacing of 2 and 1 μm in the longitudinal and transverse direction, respectively. This resulted in 49 columns and 14 rows of t-tubules. Spacing of the t-tubules was adjusted according to the strain described above.

We rendered cross-sections of the synthetic cells in 2D images at an isotropic spatial resolution of 160 pixels/μm. Images were convolved with a 2D
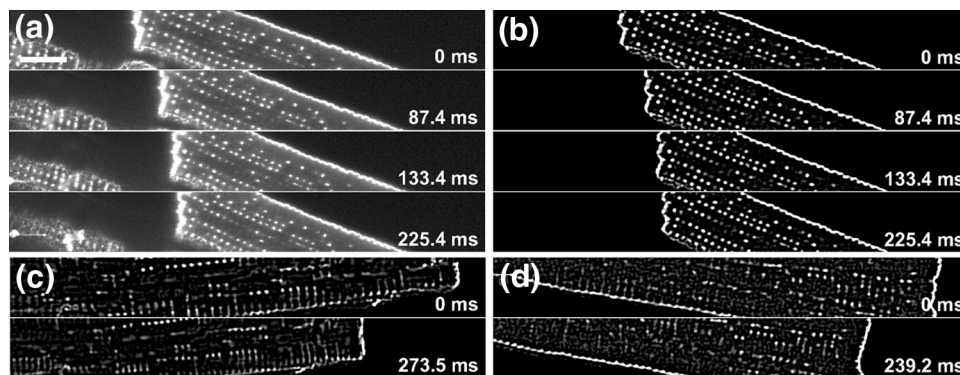
FIGURE 1. Raw and preprocessed Di-8-Anepps images from ventricular cardiomyocytes. (a) Raw and (b) preprocessed Di-8-Anepps images from control cell at different times during contraction. Preprocessed images of (c) control cell/Iso and (d) DHF cell at 0 ms and at peak contraction. Scale bar in (a) applies to (b), (c) and (d): 10 μm.
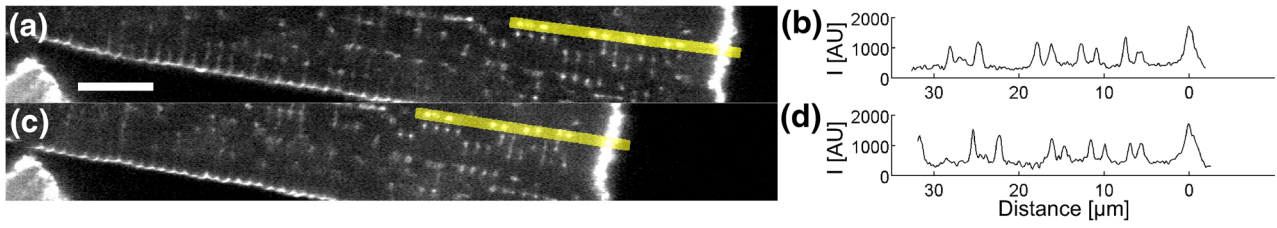
FIGURE 2. Example of manual strain measurement. (a) Cell at rest with line of interest along longitudinal axis of cell starting at cell end. (b) Intensity profile of line shown in (a). (c) Line of interest drawn in cell at peak contraction. (d) Intensity profile of line shown in (c). Scale bar in (a) applies to (b): 10 μm.

Gaussian filter (208 × 208 pixels, $\sigma_x = \sigma_y = 0.5\ \mu$m). Subsequently, the images were down-sampled to a resolution of 10 pixels/μm.

Overall, five synthetic cells were created. Two complete cells were rendered, one at 0° and one at 10° rotation. Three cropped cells were rendered in an image with a size of 128 × 1024 pixels. One of these cropped cells had 0° rotation, while the other two had a 5° rotation. One of the cropped cells with 5° rotation was rendered as a de-tubulated cell. The de-tubulated cell had all t-tubules within 10 μm of the cell end removed.

Automated Strain Measurement

Non-Rigid Image Registration

Our approach for strain measurement in image sequences from contraction cells is based on establishing a transformation Y, which registers a reference image $\mathbf{I_{ref}}$ to a deformed image $\mathbf{I_{def}}$. To register consecutive images in the image sequences we applied a previously developed efficient method for non-rigid image registration based on B-splines.[19] Here, the transformation for a control point mesh was obtained by minimizing the cost of image registration $C_{\text{Registration}}$ comprising four cost terms:

$$C_{\text{Registration}} = C_{\text{SSD}} + \psi_{\text{Be}}C_{\text{Be}} + \psi_{\text{Le1}}C_{\text{Le}_1} + \psi_{\text{Le2}}C_{\text{Le}_2} \quad (4)$$

with cost related to image similarity C_{SSD}, bending C_{Be}, and linear elasticity, C_{Le_1} and C_{Le_2}, as well as the weighting factors for their respective cost terms ψ_{Be}, ψ_{Le1}, and ψ_{Le2}. Full detail on the non-rigid image registration method and cost terms is provided in the supplemental material.

Strain Calculation

From the control point grid transformation, we calculated the displacement field $\mathbf{u}$:

$$\mathbf{u} = \mathbf{\theta}' - \mathbf{\theta}, \quad (5)$$

where $\mathbf{\theta}$ and θ' are the original and deformed control point positions, respectively. Spacing of the control point grid in all presented studies was 1 μm in x- and y-direction.

From the displacement field we calculated Cauchy's strain tensor $\mathbf{\epsilon}$ at each control point:

$$\mathbf{\epsilon} = \frac{1}{2}\left((\nabla\mathbf{u})^T + \nabla\mathbf{u}\right) = \begin{pmatrix} \frac{\partial u_x}{\partial x} & \frac{1}{2}\left(\frac{\partial u_x}{\partial y} + \frac{\partial u_y}{\partial x}\right) \\ \frac{1}{2}\left(\frac{\partial u_x}{\partial y} + \frac{\partial u_y}{\partial x}\right) & \frac{\partial u_y}{\partial y} \end{pmatrix} \quad (6)$$

with the gradient operator ∇. This strain tensor was then rotated into the coordinate system of the myocyte, which allowed us to determine the longitudinal strain $\epsilon_{\text{Long}} = \epsilon_{11}$ and the transverse strain $\epsilon_{\text{Trans}} = \epsilon_{22}$.

For parameter sensitivity studies and stochastic parameter optimization we assessed total cost of a transformation obtained by non-linear image registration by a cost C_{IMG} related to image similarity:

$$C_{\text{IMG}} = \frac{1}{N}\sum_{n=1}^{N}(\mathbf{I_{ref}}(n) - \mathbf{I_{def}}(n))^2 \quad (7)$$

and a second cost term C_σ determined by the standard deviation σ of the longitudinal strain ϵ_{Long} and the transverse strain ϵ_{Trans}:

$$C_\sigma = \sigma\left(\epsilon_{\text{Long}}\right)^2 + \sigma\left(\epsilon_{\text{Trans}}\right)^2. \quad (8)$$

For these cost calculations only image values and strains within a region of interest were considered. These two terms determine the total cost C_{Total}:

$$C_{\text{Total}} = \sqrt{C_{\text{IMG}} + \gamma C_\sigma} \quad (9)$$

with the weighting factor γ.

The algorithm calculated incremental strain ϵ^f at each control point, which is defined as the strain (longitudinal or transverse) between image f and $f+1$. To obtain the total strain, ϵ_T^f, at image f, from initial image $f = 1$, we integrated mean incremental strains ϵ^f using
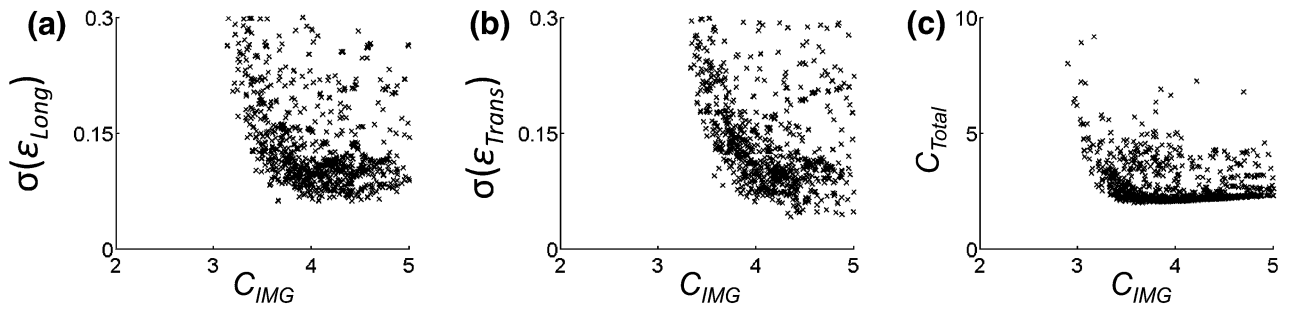
FIGURE 3. Parameter sensitivity study on cropped synthetic cell. (a) Scatter plot of standard deviation of longitudinal strain $\sigma(\varepsilon_{\text{Long}})$ vs. cost of image similarity C_{IMG}. (b) Scatter plot of standard deviation of transverse strain $\sigma(\varepsilon_{\text{Trans}})$ vs. C_{IMG}. (c) Scatter plot of total cost C_{Total} vs. C_{IMG}.

$$\varepsilon_T^f = \left(\sum_{i=2}^{f} \varepsilon^{i-1} \left(1 + \varepsilon^i \right) \right) - 1. \qquad (10)$$

Parameter Sensitivity

In order to investigate how weights of registration costs affect the image registration results and strain calculations we designed a parameter sensitivity study. We varied the input parameters, in particular, weights for the bending energy and two linear elasticity terms. Weights of bending cost explored were 10^{-1}, 10^{-2}, ..., 10^{-8}. Weights of both linear elasticity costs explored were 10^{0}, $10^{-0.25}$, $10^{-0.5}$, ..., 10^{-4}. Overall, each parameter sensitivity study led to a total of 2312 image registrations.

Parameterization Based on Stochastic Optimization

We applied an approach for stochastic parameter optimization to minimize total cost of image transformation and the associated strain (Eq. 9). In previous work, we developed this approach for parameterization of models of ion channels.[1] The approach iteratively evaluates variants of input parameters ψ_{Be}, ψ_{Le1}, and ψ_{Le2} for registration of image pairs. Initial values for optimization were determined by the parameter sensitivity study described above on sample frames from image sequences. The algorithm then generates 80 parameter sets with random perturbations (10–1000%) from the initial parameter values constrained by the ranges $[10^{-8}\ 10^{-1}]$ for the weights of bending cost and $[10^{-4}\ 10^{-0}]$ for weights of the linear elasticity costs. The cost C_{Total} for each parameter set was calculated. Two parameter sets yielding the smallest C_{Total} were used as initial values for the next iteration. Five iterations were performed resulting in 400 calculations for each image pair. The parameter set with minimal C_{Total} after the 5th iteration was kept and the resulting transformation was used for subsequent analyses.

Implementation

Image processing and the strain measurement algorithm were implemented in MATLAB 2014a (Mathworks, Natick, NA). We used a C++ implementation of a method for non-rigid image registration (NiftyReg, v1.39).[17] We provide further detail on the implementation in the Supplemental Material.

RESULTS

Evaluation of Algorithm

Parameter Sensitivity Study on Synthetic Cells

We performed an extensive parameter sensitivity study to investigate properties of non-rigid image registration for strain measurement in cardiomyocytes. We used synthetic cells with a homogeneous strain distribution for this purpose. The sensitivity study revealed that in these cells, minimal C_{IMG}, i.e. maximal similarity of the reference and deformed image, is not associated with minimal $\sigma(\varepsilon_{\text{Long}})$ and $\sigma(\varepsilon_{\text{Trans}})$ (Figs. 3a and 3b), indicating heterogeneity of strain distributions after image registration. Because strain was homogeneous in the synthetic cells, the measured heterogeneity suggests a general issue in the application of the described non-rigid image registration approach for strain measurement. We thus developed a simple cost function (total cost C_{Total}, Eq. 9) to include measures of strain heterogeneity. Investigating this cost function (Fig. 3c) revealed that various parameter sets yield small C_{Total} while maintaining a small C_{IMG}.

We present cost terms C_{IMG}, C_σ, and C_{Total} resulting from image registration of a synthetic cell in Fig. 4. Cost distributions were a complex function of weighting parameters. Cost distributions exhibited local maxima and minima, thus hindering traditional optimization approaches for parameter identification. However, various parameter combinations yielded small C_{Total}.
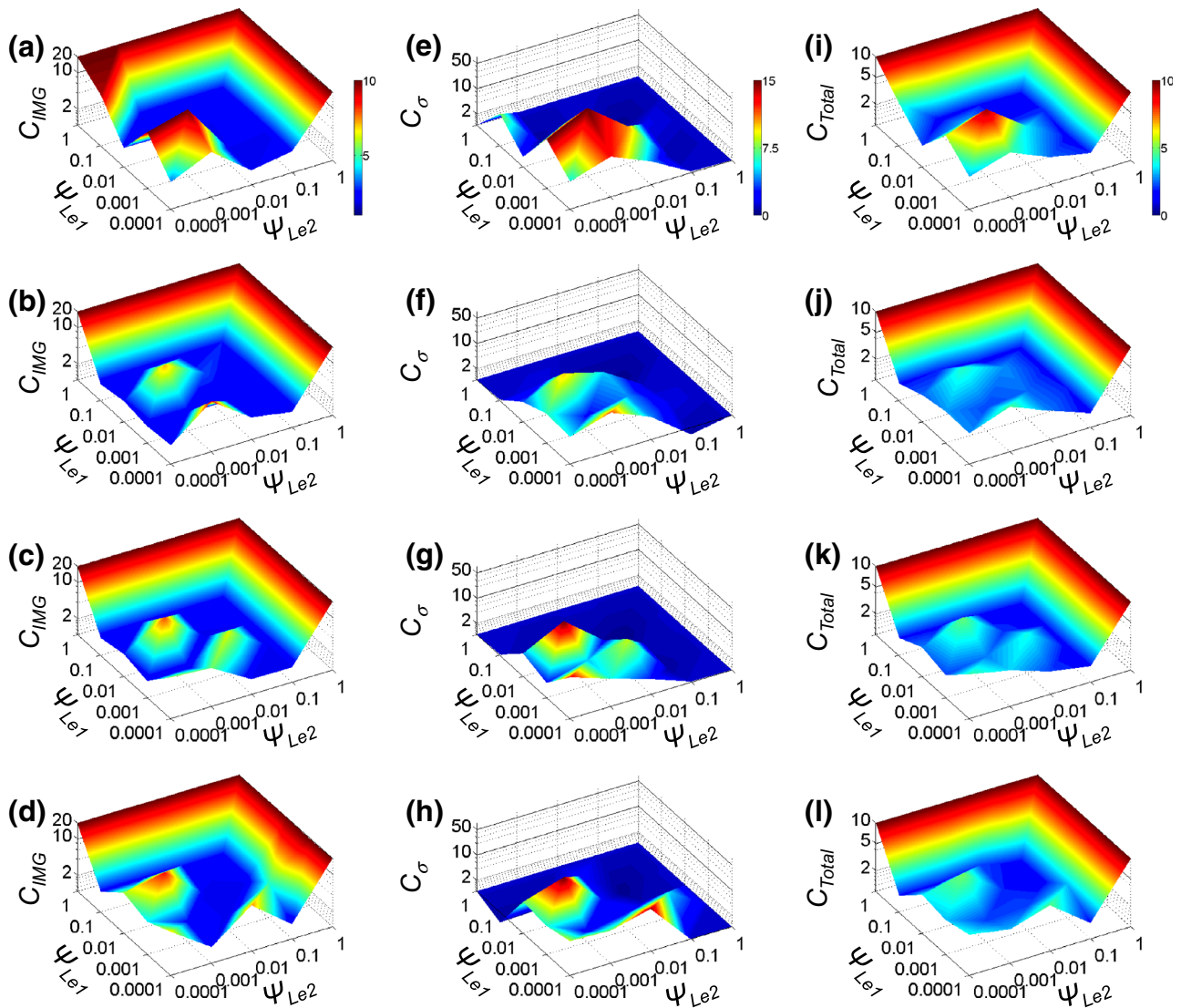
FIGURE 4. Parameter sensitivity study on cropped synthetic cell. (a–d) Costs related to image similarity C_{IMG}. (e–h) Costs related to standard deviation of strain C_{σ}. (i–l) Total cost C_{Total}. Bending weights ψ_{Be} were set to (a, e, i) 10^{-5}, (b, f, j) 10^{-6}, (c, g, k) 10^{-7} and (d, h, l) 10^{-8}. Colorbars in (a, e, and i) apply to all plots of the respective costs.

Strain Measurement in Synthetic Cells

We studied reliability of strain detection in various synthetic cells. Minimizing the cost function described in Eq. 9, we studied strain measurement in the complete, unrotated synthetic cell (Fig. 5). A calculated displacement field for -10% strain is shown in Fig. 5b. Resulting displacement in long-axis (x) direction were 5 and -5 μm at the left and right cell end, respectively. The displacement amplitude decays linearly to 0 μm at the center of the cell. Short-axis (y) displacements also increased linearly from -0.5 pixels to 0.5 μm from the top to bottom of the cell. The measured displacements are consistent with the displacements specified for a homogeneous ε_{Long} and ε_{Trans} of -10 and $+5.4\%$. Cauchy's strain tensor $\boldsymbol{\varepsilon}$ was

then calculated using this displacement field (Eq. 6). A discretized map of the resulting strain tensors is shown in Fig. 5c. Strain tensors were approximately uniform within the cell, but strain outside of the cell varied significantly. However, our analyses were restricted to the cell interior.

Figure 5d shows the incremental strains calculated for images with decreasing ε_{Long} to -10% and increasing ε_{Trans} to 5% in 10 steps. Solid lines present results of stochastic optimization (described above). The black plus signs and squares present strain calculations with constant input parameters, which were optimized for the first and second images. In this cell differences between the static registration and the stochastic optimization approach were small. Each
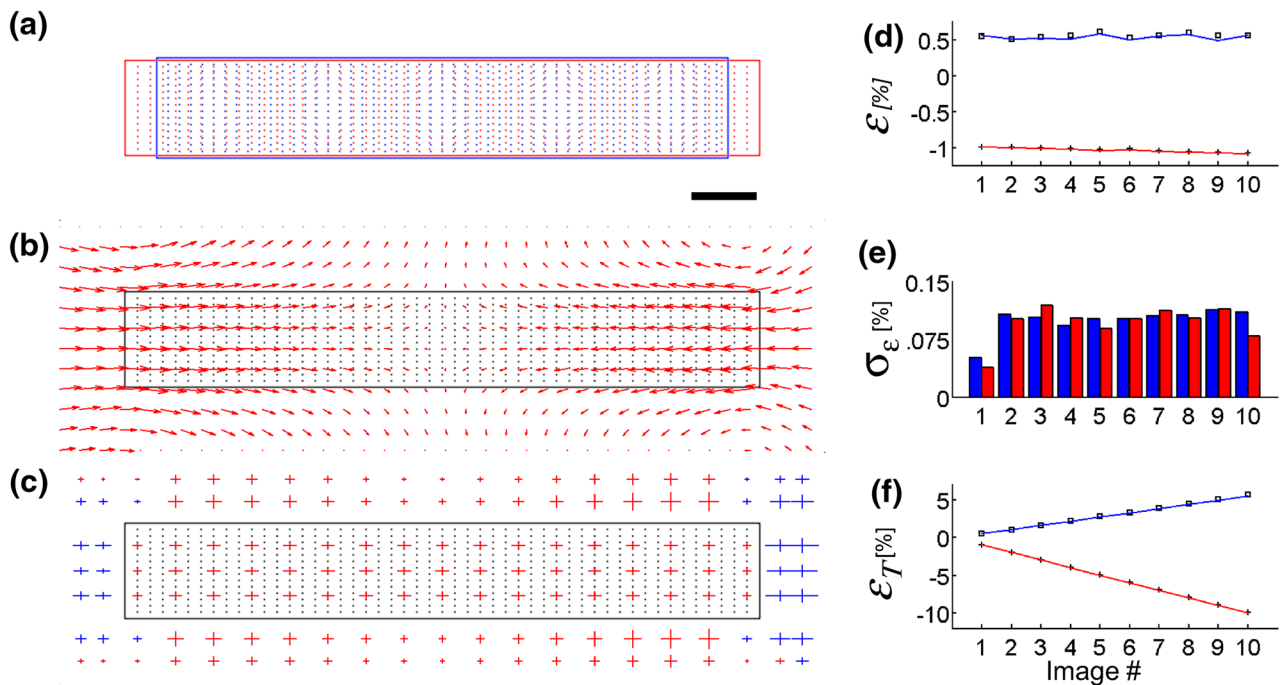
FIGURE 5. Strain measurement in complete, unrotated synthetic cell. (a) Cell at 0% (red) and −10% ε_{Long} (blue). (b) Displacements and (c) strain tensors associated with −10% ε_{Long} overlaid on cell at 0% ε_{Long}. Red and blue color represents shortening and dilation, respectively, along the *x*-axis. (d) Calculated strain for each frame using a stochastic optimization approach (red and blue) vs. a static parameter approach (square box and +). Transverse strain shown in blue and square box, longitudinal strain in red and +. (e) Standard deviation of the longitudinal (red) and transverse (blue) strain for each frame. (f) Total strain using the stochastic optimization approach (red and blue) vs. a static parameter approach (square box and +). Transverse strain shown in blue and square box, longitudinal strain in red and +. Scale bar in (a) applies to (b) and (c): 10 μm.

image in the sequence describes cell deformation for a specific strain vs. the original image, thus ε_{Long} is not constant at 1%. The minor negative slope is in agreement with the specified ε_{Long}.

We assessed homogeneity of ε_{Long} and ε_{Trans} within the cell (Fig. 5e). Standard deviation of strain from registration of images 1 and 2 is smallest since optimal parameter values were derived from the parameter sensitivity study using these images. Overall the standard deviation is smaller than 0.1% for both strains. We calculated the total strain (Eq. 10, Fig. 5f). ε_{Long} decreased linearly from −1 to −10% in image 1–10 while ε_{Trans} increased from 0.5 to 5.4%, which is consistent with the strain specified for the synthetic cell.

Strain Measurements in Rotated and Partial Synthetic Cells

We next assessed reliability of the strain measurement algorithm under realistic conditions for cell imaging. We considered that imaged cells exhibit various angles and are only partially in the field of view (Fig. 6). We investigated models of a complete and rotated (Fig. 6a), cropped and unrotated (Fig. 6d), cropped and rotated (Fig. 6g), and cropped, rotated and partially de-tubulated cell (Fig. 6j). Incremental strains using the stochastic parameter optimization

approach and static parameters for each of these configurations are shown in Figs. 6b, 6e, 6h, and 6k. Total strains are presented in Figs. 6c, 6f, 6i, and 6l. While the stochastic optimization approach yielded expected results for all cell configurations, using static parameters led to several cases of inaccurate measurements. This is most apparent in Figs. 6e and 6k. Overall these studies indicate that strain measurement based on stochastic parameter optimization is superior vs. measurement applying static parameters.

A summary of strain measurements for all synthetic cells is presented in Table 1. These data show that errors between specified and measured strains are small even using images of cells that were cropped, rotated, and de-tubulated. Errors for ε_{Long} and ε_{Trans} were up to 0.1 and 0.3%, respectively. Importantly, the summary suggests that the developed stochastic parameter optimization approach was able to capture the strain in a reliable manner. Furthermore the studies indicate that reliability of strain detection is not affected by limited field of view and density of t-system.

Strain Measurements in Ventricular Cardiomyocytes

We investigated the approach of stochastic parameter optimization introduced above in image sequences

from rapid scanning of contracting ventricular myocytes (Fig. 1 and Supplemental Fig. 1). In particular, we explored if the approach is capable of detecting heterogeneity of regional contraction. For this purpose, we binned cells into 10 μm regions from the longitudinal cell end and evaluated cost terms within these regions. We measured regional incremental (Figs. 7a, 7d, and 7g) and total strains (Figs. 7b, 7e, and 7h) for a control cell in 4 mM Ca^{2+}, a control cell in 4 mM Ca^{2+} with isoproterenol, and a DHF cell in 2 mM Ca^{2+}. We then analyzed the regional transients

of ε_{Long} and ε_{Trans}. In Table 2 we summarized quantitative data from these analyzes.

The maximal incremental ε_{Long} and its timing varied between all three cells. Time of maximal incremental ε_{Long} was 32.2, 23.0, and 55.2 ms for the control, control/Iso and DHF cell, respectively. Here, times are related to first appearance of calcium signal, which occurs shortly after pacing. Peak ε_{Long} and time to peak ε_{Long} varied among the 3 cells: -13.7% at 170.2 ms for control, -25.7% at 253 ms for control cell/Iso, and -11.0% at 271.4 ms for the DHF cell.
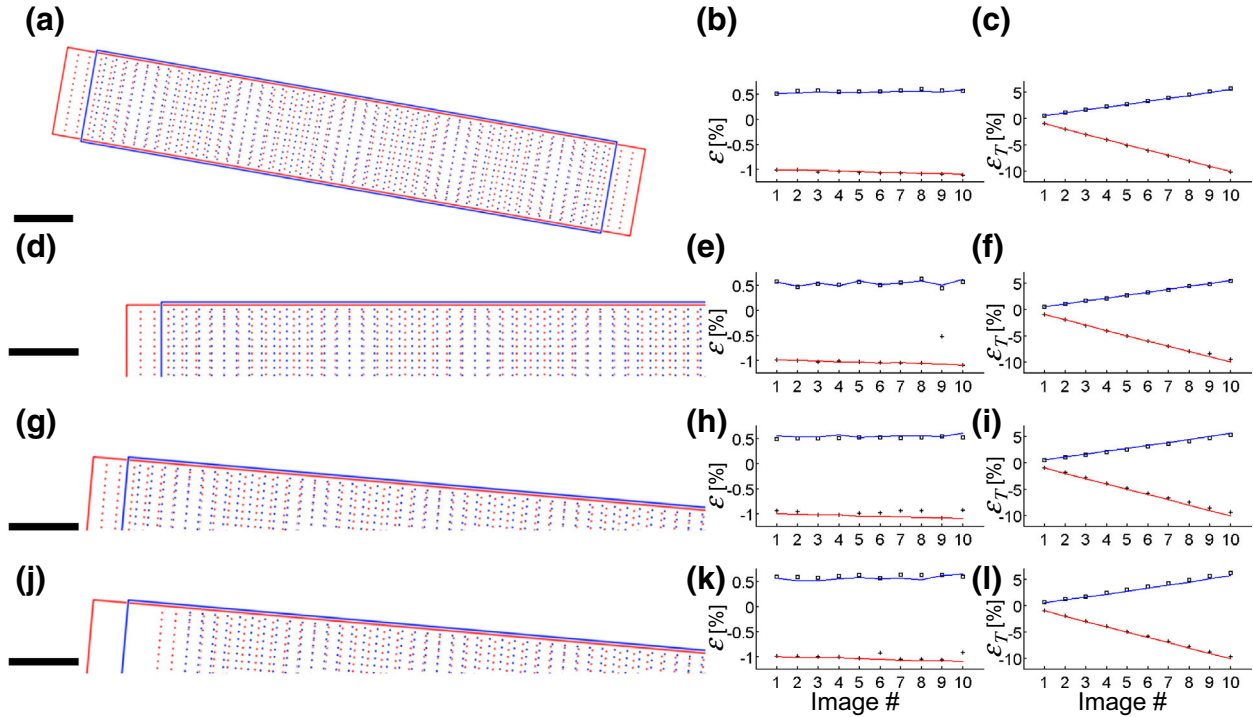
FIGURE 6. Strain measurement in synthetic cells. (a, d, g, j) Images of cells with 0% (red) and -10% ε_{Long} (blue). (a) Fully padded synthetic cell rotated by 10°. (d) Cropped synthetic cell with no rotation. (g) Cropped synthetic cell rotated by 5°. (j) Cropped synthetic cell rotated by 5° and de-tubulated within 10 μm of cell end. (b, e, h, k) Incremental strain and (c, f, i, l) total strain for each frame in the longitudinal (red) and transverse (blue) directions. Results from the stochastic parameter optimization approach (red and blue lines) are contrasted with results from the static parameter approach (square box and +). Scale bars: 10 μm.

TABLE 1. Quantitative results of strain measurement in synthetic cells.

Cell	Set ε_{Long} (%)	Measured ε_{Long} (%)	$\Delta\varepsilon_{Long}$ (%)	Set ε_{Trans} (%)	Measured ε_{Trans} (%)	$\Delta\varepsilon_{Trans}$ (%)
Complete	-10.0	-9.9	0.1	5.4	5.4	0.0
Complete and rotated	-10.0	-10.1	0.1	5.4	5.4	0.0
Cropped	-10.0	-10.0	0.0	5.4	5.5	0.1
Cropped and rotated	-10.0	-10.0	0.0	5.4	5.6	0.2
Cropped, rotated, and de-tubulated	-10.0	-10.1	0.1	5.4	5.7	0.3

Corresponding cells are shown in Figs. 4a, 5a, 5d, 5g, and 5j. Set ε_{Long} is the strain specified for the synthetic cells. Measured ε_{Long} is peak longitudinal strain measured using stochastic parameter optimization. $\Delta\varepsilon_{Long}$ is the difference between the mean of Set ε_{Long} and Measured ε_{Long}. Set ε_{Trans} is the specified transverse strain calculated using Eq. 3. Measured ε_{Trans} is the peak measured transverse strain using stochastic parameter optimization. $\Delta\varepsilon_{Trans}$ is the difference between Set ε_{Trans} and Measured ε_{Trans}.

Both control cells did not display major differences between the four regions over the course of contraction. However, the DHF cell exhibited a ~40% reduction in peak ε_{Long} within 0–10 μm when compared to the other regions, which showed only minor differences of peak ε_{Long}.

Comparison of measured ε_{Long} and ε_{Trans} revealed an inverse relationship. In all cells, decreased ε_{Long} was associated with increased ε_{Trans}. Similar as for ε_{Long} the DHF cell exhibited a large heterogeneity of ε_{Trans}, with small values found at the cell end. In all cells, predicted ε_{Trans} (Eq. 3) was not in agreement with measured ε_{Trans}.

To evaluate reliability of the developed approach we compared calculated results with results from manual strain measurement. Results from manual strain mea-
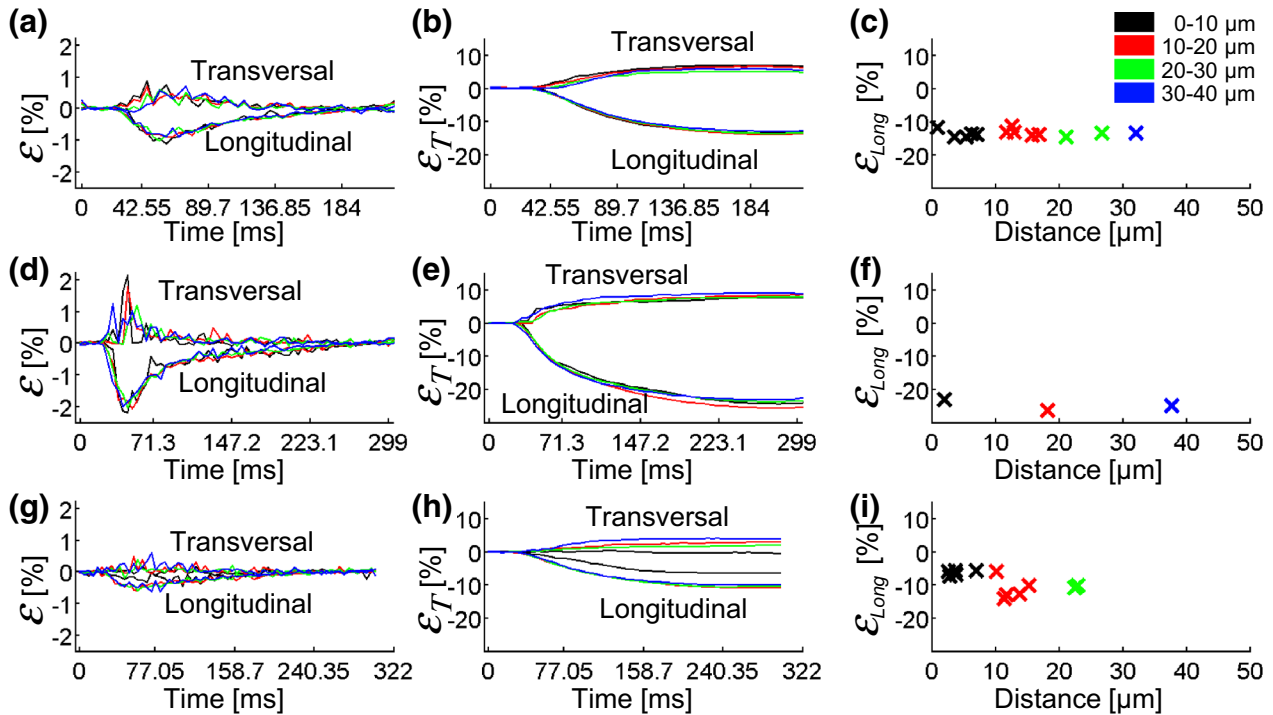
FIGURE 7. Strain measurement in ventricular cardiomyocytes. (a, d, g) Incremental and (b, e, h) total ε_{Long}. (c, f, i) Manual measurement of ε_{Long}. Calculated ε_{Long} in (a–c) control cell, (d–f) control cell/Iso and (g–i) DHF cell.

TABLE 2. Quantitative results of strain algorithm on ventricular cardiomyocytes.

Cell	Range (μm)	Manual ε_{Long} (%)	Measured ε_{Long} (%)	$\Delta\varepsilon_{Long}$ (%)	Predicted ε_{Trans} (%)	Measured ε_{Trans} (%)	$\Delta\varepsilon_{Trans}$ (%)
Control	0–10	-13.8 ± 1.2 ($n = 5$)	-13.5	0.3	7.5	6.9	0.6
	10–20	-13.2 ± 1.1 ($n = 5$)	-14.0	0.8	7.8	6.6	1.2
	20–30	-14.0 ± 0.8 ($n = 2$)	-13.7	0.3	7.6	5.1	2.5
	30–40	-13.5 ($n = 1$)	-13.0	0.5	7.2	5.8	1.4
Control/Iso	0–10	-23.1 ($n = 1$)	-24.4	1.3	15.0	7.5	7.5
	10–20	-26.5 ($n = 1$)	-25.7	0.8	16.0	8.3	7.7
	20–30	–	-23.7	–	14.5	7.8	6.7
	30–40	-25.0 ($n = 1$)	-23.1	1.9	14.1	9.0	5.1
DHF	0–10	-6.3 ± 0.8 ($n = 5$)	-6.5	0.2	3.4	-0.3	3.7
	10–20	-12.0 ± 1.8 ($n = 5$)	-11.0	1.0	6.0	2.9	3.1
	20–30	-10.5 ± 0.6 ($n = 2$)	-10.6	0.1	5.8	1.7	4.1
	30–40	–	-10.0	–	5.4	3.8	1.6

Control, Control/Iso and DHF cells are shown in Figs. 1b, 1c, and 1d respectively. Manual ε_{Long} is the average of the manual strain calculation for each region, reported as mean $\pm$ standard deviation with the number of points, n, measured for the region. Measured ε_{Long} is the peak longitudinal strain measured using stochastic parameter optimization. $\Delta\varepsilon_{Long}$ is the difference between the mean of Manual ε_{Long} and Measured ε_{Long}. Predicted ε_{Trans} is the transverse strain calculated by Eq. 3 using Measured ε_{Long}. Measured ε_{Trans} is the peak measured transverse strain using stochastic parameter optimization. $\Delta\varepsilon_{Trans}$ is the difference between Predicted ε_{Trans} and Measured ε_{Trans}.

surements are plotted in Figs. 7c, 7f and 7i. Control cells exhibited homogeneous ε_{Long} within all regions, while the DHF cell showed decreased ε_{Long} within 0–10 μm of the cell end. For all cells and regions, the difference between calculated and measured ε_{Long} was small (Table 2).

DISCUSSION

In this study, we introduced and evaluated an approach for measurement of regional strain in image sequences of contracting cardiac myocytes acquired with rapid scanning confocal microscopy. The approach is based on non-rigid image registration and calculation of strain from registered images. In contrast to previously developed approaches the approach is capable of measurement of longitudinal and transverse strain at microscopic scale in 2-dimensions.

We applied synthetic cells to develop and extensively evaluate the approach. We further explored the approach in a control cardiomyocyte, a cell with drug-increased contractility, and a cell from an animal model of heart failure. The presented analysis of measured strain profiles indicate that the approach facilitates quantitative characterization of contractility of cardiac myocytes. In particular, application of the approach allowed us to comprehensively quantify cell contractility and regional heterogeneity of cell contraction in heart failure cells. Contraction in control cells with or without adrenergic stimulation was regionally homogenous. Adrenergic stimulation was associated with accelerated and largely increased shorting (more negative ε_{Long}) vs. control. DHF was associated with delayed and decreased shortening (less negative ε_{Long}), which is consistent with previous measurements,[7] as well as regional heterogeneity of contraction, which has not been reported before.

While it is well established that various types of heart failure are associated with microstructural heterogeneity of cardiomyocytes,[13,14] effects of this heterogeneity on regional contraction have not been studied. In our previous work, we found regional structural remodeling, in particular, de-tubulation at cell ends in DHF,[13] which might explain the finding of reduced shortening detected by the developed approach. Some degree of de-tubulation at the cell end is also visible in the studied DHF cardiomyocyte (Fig. 1d). The presented development was motivated by our interest in effects of this heterogeneity on contraction. We suggest that the developed approach provides researchers with a crucial tool to investigate regional heterogeneity of contraction. Additionally,

the approach provides additional information on strain vs. previously employed methods. We anticipate that improved description of the mechanical properties of contracting myocytes using these measurements will lead to further development and evaluation of computational models of myocyte contraction.[20]

In initial studies with synthetic cells we found that various choices of parameters for image registration were associated with high similarity of registered images, but strains measured from these registrations varied widely within the cell (Fig. 3). Thus, it is not possible to use them without modification for reliable measurement of regional cellular strain. We added a cost term to restrict the regional strain variability, while maintaining high similarity of registered images (Eq. 9). The results of the parameter sensitivity study show that even this cost term yields many maxima and minima. This hinders the ability of traditional methods for minimization to converge and find a global minimum. Thus we implemented a stochastic optimization approach using a total cost term for parameterization of image registration, which was crucial to avoid issues resulting from static parameterization of the image registration (e.g. Figs. 6e and 6g). We investigated several variants of synthetic cells including cells that were cropped and rotated within the image similar to what is seen in our imaging sequences from rapid scanning confocal microscopy (Fig. 1 and Supplemental Fig. 1). Strain measurements from those cells and a synthetic cell with sparse t-system suggested that the developed stochastic optimization approach is robust with respect to imaging conditions and microstructural variation of cells.

Our approach provides information on transverse strain in addition to the conventionally measured longitudinal strain. None of the methods developed over the last 3 decades described in the "Introduction" section were capable of or attempted to extract this information. The measured strain yielded an inverse relationship between ε_{Long} and ε_{Trans}, which reflects volume preservation that is commonly assumed during myocyte contraction. However, the prediction of ε_{Trans} based on ε_{Long} and assuming volume preservation and transversely isotropic mechanical properties (Eq. 3) yielded larger values than our measurement of ε_{Trans}. This might be explained by transversely anisotropic dilation of contracting cells. Commonly, isolated cells are lying flat on the glass slide, i.e. cell height is smaller than width. The imaging section is parallel to the 1st and 2nd principal axis of myocytes. To account for volume preservation and our resulting measurements, ε_{Trans} would be required to be larger along the 3rd than the 2nd principal axis. Anisotropy in the transverse

strain could be caused by anisotropic mechanical properties of cells resulting from cellular microstructure, for instance, by anisotropic arrangement of the cytoskeleton. A recent modeling study using isotropic material properties estimated that during shortening the magnitude of longitudinal strain inside the cell is about two times the magnitude of both transverse strains.[25] This study supports our hypothesis that anisotropic mechanical properties of cells are required to explain our finding of transversally anisotropic strains. While we cannot relate our findings to the established anisotropic strain and stress distribution in the whole heart,[20] we believe that our studies provide a foundation for investigations of this relationship.

We evaluated our approach for strain measurement using manual detection in image sequences during contraction of cardiac myocytes. Manual strain detection was based on analyzes of images from cells at rest and peak contraction. While manually measured and calculated strains were in agreement for all investigated cells, we note several major difficulties with the approach for manual measurements. First of all, small differences of peak image intensity detection strongly affect strain calculations. In particular at the cell end, local intensity profiles might exhibit peaks that are not corresponding to a single location, but produced by overlay of several structures that are displaced during contraction. A further issue is related to structures that move into and out of the field of view. Here, correspondence of profiles at rest and in contraction cannot be established.

LIMITATIONS

We discussed limitations of our methods for cell labeling and rapid scanning confocal microscopy previously.[13,28] In short, confocal microscopy has a limited spatial and temporal resolution. Imaged structures, i.e. Di-8-anepps labeled sarcolemma, are thin (~5 nm), thus images of those structures are strongly affected by the point-spread function of the imaging system.[8] We did not explore methods of image deconvolution to reduce this artifact. We do not believe that limited temporal resolution affected the presented strain measurements, because inspection of the strain profiles caused by contraction did not indicate frequency components beyond what can be covered by a sampling of 4.6 ms/frame based on the sampling theorem. Also, images from confocal microscopy are affected by several sources of noise. To reduce effects of noise on strain detection we applied filters for noise reduction. A limitation of our approach is its dependence on t-system distribution as structural markers within the cell. Alternative labeling

approaches in living cells are currently in development and include fluorescent markers of intracellular organelles, in particular, mitochondria and sarcomeric proteins.[10] A limitation of our study is that we investigated only contraction and neglected relaxation. While, this was motivated by our focus on characterizing contractility of diseased cells, we do not expect issues with applying the approach for measurements of cell relaxation. We evaluated our approach using isolated cells. However, in principle, it is possible to obtain similar image data from tissue and isolated heart preparation indicating that our approach can be useful for studies of tissue and heart contractility. While our image data also includes information on calcium signaling, we did not attempt to establish a relationship between calcium and contraction. In our previous work, we present calcium transients from the applied animal models and methods for their analyzes.[13,21] We suggest that integration of these methods with the presented approach will lead to novel insights into the subcellular relationship between calcium and contraction. An additional limitation is that isolated cardiomyocytes are known to exhibit decreased contractility due to the lack of adrenergic stimulation, diastolic stretch, and other inotropic factors found in vivo. For this reason, $[Ca^{2+}]_0$ was increased to above physiological concentrations in order to obtain larger and apparently more physiological strains.

ELECTRONIC SUPPLEMENTARY MATERIAL

The online version of this article (doi: 10.1007/s10439-016-1593-7) contains supplementary material, which is available to authorized users.

REFERENCES

[1]Abbruzzese, J., F. B. Sachse, M. Tristani-Firouzi, and M. C. Sanguinetti. Modification of hERG1 channel gating by Cd2 + . *J. Gen. Physiol.* 136:203–224, 2010.

[2]Aiba, T., G. G. Hesketh, A. S. Barth, T. Liu, S. Daya, K. Chakir, V. L. Dimaano, T. P. Abraham, B. O'Rourke, F. G. Akar, D. A. Kass, and G. F. Tomaselli. Electrophysiological consequences of dyssynchronous heart failure and its restoration by resynchronization therapy. *Circulation* 119:1220–1230, 2009.

[3]Bers, D. M. Cardiac excitation-contraction coupling. *Nature* 415:198–205, 2002.

[4]Bub, G., P. Camelliti, C. Bollensdorff, D. J. Stuckey, G. Picton, R. A. Burton, K. Clarke, and P. Kohl. Measurement and analysis of sarcomere length in rat cardiomyocytes in situ and in vitro. *Am. J. Physiol. Heart Circ. Physiol.* 298:H1616–H1625, 2010.

[5]Chakir, K., S. K. Daya, T. Aiba, R. S. Tunin, V. L. Dimaano, T. P. Abraham, K. M. Jaques-Robinson, E. W. Lai, K. Pacak, W. Z. Zhu, R. P. Xiao, G. F. Tomaselli, and D. A. Kass. Mechanisms of enhanced beta-adrenergic reserve from cardiac resynchronization therapy. *Circulation* 119:1231–1240, 2009.

[6]Chakir, K., S. K. Daya, R. S. Tunin, R. H. Helm, M. J. Byrne, V. L. Dimaano, A. C. Lardo, T. P. Abraham, G. F. Tomaselli, and D. A. Kass. Reversal of global apoptosis and regional stress kinase activation by cardiac resynchronization. *Circulation* 117:1369–1377, 2008.

[7]Chakir, K., C. Depry, V. L. Dimaano, W. Z. Zhu, M. Vanderheyden, J. Bartunek, T. P. Abraham, G. F. Tomaselli, S. B. Liu, Y. K. Xiang, M. Zhang, E. Takimoto, N. Dulin, R. P. Xiao, J. Zhang, and D. A. Kass. Galphas-biased beta2-adrenergic receptor signaling from restoring synchronous contraction in the failing heart. *Sci. Transl. Med.* 3:100ra88, 2011.

[8]Diaspro, A. Confocal and Two-Photon Microscopy: Foundations, Applications, and Advances. New York: Wiley-Liss, 2002.

[9]Goldman, Y. E. Measurement of sarcomere shortening in skinned fibers from frog muscle by white light diffraction. *Biophys. J.* 52:57–68, 1987.

[10]Goldman, R. D., J. Swedlow, and D. L. Spector. Live Cell Imaging: A Laboratory Manual (2nd ed.). Cold Spring Harbor, N.Y.: Cold Spring Harbor Laboratory Press, 2010.

[11]Harris, P. J., D. Stewart, M. C. Cullinan, L. M. Delbridge, L. Dally, and P. Grinwald. Rapid measurement of isolated cardiac muscle cell length using a line-scan camera. *IEEE Trans. Biomed. Eng.* 34:463–467, 1987.

[12]Lecarpentier, Y., J. L. Martin, V. Claes, J. P. Chambaret, A. Migus, A. Antonetti, and P. Y. Hatt. Real-time kinetics of sarcomere relaxation by laser diffraction. *Circ. Res.* 56:331–339, 1985.

[13]Li, H., J. G. Lichter, T. Seidel, G. F. Tomaselli, J. H. Bridge, and F. B. Sachse. Cardiac resynchronization therapy reduces subcellular heterogeneity of ryanodine receptors, T-tubules, and Ca2 + sparks produced by dyssynchronous heart failure. *Circ Heart Fail.* 8:1105–1114, 2015.

[14]Lichter, J. G., E. Carruth, C. Mitchell, A. S. Barth, T. Aiba, D. A. Kass, G. F. Tomaselli, J. H. Bridge, and F. B. Sachse. Remodeling of the sarcomeric cytoskeleton in cardiac ventricular myocytes during heart failure and after cardiac resynchronization therapy. *J. Mol. Cell. Cardiol.* 72:186–195, 2014.

[15]London, B., and J. W. Krueger. Contraction in voltage-clamped, internally perfused single heart cells. *J. Gen. Physiol.* 88:475–505, 1986.

[16]McNary, T. G., J. H. Bridge, and F. B. Sachse. Strain transfer in ventricular cardiomyocytes to their transverse tubular system revealed by scanning confocal microscopy. *Biophys. J.* 100:L53–L55, 2011.

[17]Modat, M., G. R. Ridgway, Z. A. Taylor, M. Lehmann, J. Barnes, D. J. Hawkes, N. C. Fox, and S. Ourselin. Fast free-form deformation using graphics processing units. *Comput. Methods Programs Biomed.* 98:278–284, 2010.

[18]Philips, C. M., V. Duthinh, and S. R. Houser. A simple technique to measure the rate and magnitude of shortening of single isolated cardiac myocytes. *IEEE Trans. Biomed. Eng.* 33:929–934, 1986.

[19]Rueckert, D., L. I. Sonoda, C. Hayes, D. L. Hill, M. O. Leach, and D. J. Hawkes. Nonrigid registration using free-form deformations: application to breast MR images. *IEEE Trans. Med. Imaging* 18:712–721, 1999.

[20]Sachse, F. B. Computational Cardiology: Modeling of Anatomy, Electrophysiology, and Mechanics. Berlin: Springer, 2004.

[21]Sachse, F. B., N. S. Torres, E. Savio-Galimberti, T. Aiba, D. A. Kass, G. F. Tomaselli, and J. H. Bridge. Subcellular structures and function of myocytes impaired during heart failure are restored by cardiac resynchronization therapy. *Circ. Res.* 110:588–597, 2012.

[22]Schneider, C. A., W. S. Rasband, and K. W. Eliceiri. NIH Image to ImageJ: 25 years of image analysis. *Nat. Methods* 9:671–675, 2012.

[23]Schwab, B. C., G. Seemann, R. A. Lasher, N. S. Torres, E. M. Wulfers, M. Arp, E. D. Carruth, J. H. Bridge, and F. B. Sachse. Quantitative analysis of cardiac tissue including fibroblasts using three-dimensional confocal microscopy and image reconstruction: towards a basis for electrophysiological modeling. *IEEE Trans. Med. Imaging* 32:862–872, 2013.

[24]Seidel, T., T. Dräbing, G. Seemann, and F. B. Sachse. A semi-automatic approach for segmentation of three-dimensional microscopic image stacks of cardiac tissue. *Lect. Notes Comput. Sci.* 7945:7, 2013.

[25]Shaw, J., L. Izu, and Y. Chen-Izu. Mechanical analysis of single myocyte contraction in a 3-D elastic matrix. *PLoS ONE* 8:e75492, 2013.

[26]Steadman, B. W., K. B. Moore, K. W. Spitzer, and J. H. B. Bridge. A video system for measuring motion in contracting heart cells. *IEEE Trans. Biomed. Eng.* 35:264–272, 1988.

[27]Tameyasu, T., T. Toyoki, and H. Sugi. Nonsteady motion in unloaded contractions of single frog cardiac cells. *Biophys. J.* 48:461–465, 1985.

[28]Torres, N. S., F. B. Sachse, L. T. Izu, J. I. Goldhaber, K. W. Spitzer, and J. H. Bridge. A modified local control model for Ca2 + transients in cardiomyocytes: junctional flux is accompanied by release from adjacent non-junctional RyRs. *J. Mol. Cell. Cardiol.* 68:1–11, 2014.